文章编号：1001-9014(2020)02-0157-06

DOI:10. 11972/j. issn. 1001-9014. 2020. 02. 004

Design and cold-test of sheet beam coupled cavity slow wave structure for W-Band TWT

LU Zhi-Gang, GE Wei-Hua, WEN Rui-Dong, SU Zhi-Cheng, ZHU Mei-Ling, DING Ke-Sen, WANG Zhan-Liang, TANG Tao

(National Key Laboratory of Science and Technology on Vacuum Electronics, School of Electronic Science and Engineering, University of Electronic Science and Technology of China, Chengdu 610054, China)

Abstract: This paper presents the fabrication and cold-test of a three-slot-staggered-ladder coupled cavity slow wave structure (CC-SWS) along with high power input-output couplers and RF windows in W-band. The SWS is fed by a rectangular waveguide coupler which is made up of a three-order step-transform rectangular waveguide placed on the short edge of the input cavity. Firstly, the dispersion, interaction impedance, transmission property and beam-wave interaction are studied using the simulation method. It is shown that the traveling wave tube (TWT) with a three-slot-staggered-ladder CC-SWS is able to provide a saturation output power of more than 1000 W in the frequency range of 91~96 GHz, and the maximum saturated output power can reach 1125 W at 94 GHz. Secondly, the CC-SWS is fabricated by the high-precision CNC milling and fixed in a nonmagnetic stainless steel housing. Test results of the fabricated CC-SWS with couplers and RF-windows are presented, showing the S_{11} < -10 dB in the frequency range of 90 GHz to 100 GHz. Therefore, the three-slot-staggered-ladder CC-SWS is a promising slow wave circuit of high power W-band TWT.

Key words: traveling wave tube, W-band, three-slot-staggered-ladder, coupled cavity slow wave structure (CC-SWS), cold test

PACS: 41. 60. Bq

W波段带状注耦合腔慢波结构行波管的设计与冷测

路志刚, 葛卫华, 温瑞东, 苏志成, 朱美玲, 丁科森, 王战亮, 唐 涛

(电子科技大学 电子科学与工程学院 大功率微波电真空器件技术国防科技重点实验室,四川 成都 610054)

摘要:对W波段三槽梯形线耦合腔慢波结构(包括大功率输入输出耦合器和射频窗)的加工和冷测进行了研究。此慢波结构由一个矩形波导耦合器馈电,该耦合器由放置在输入腔短边上的三阶阶梯变换矩形波导组成。首先,利用仿真方法研究了慢波结构的色散、互作用阻抗、传输特性和注-波互作用。结果表明,采用三槽梯形线耦合腔慢波结构的行波管能够在91~96 GHz的频率范围内提供大于1 000 W的饱和输出功率,并且在94 GHz频点,饱和输出功率最大,可以达到1 125 W。其次,采用高精度数控铣床加工出三槽梯形线慢波结构,并将其固定在非磁性不锈钢外壳中。文中给出了带有耦合器和射频窗的三槽梯形线慢波系统的测试结果,表明在90 GHz到100 GHz的频率范围内,S_{11}<-10 dB。因此,三槽梯形线慢波结构在W波段大功率行波管方面具有应用前景。

关 键 词:行波管;W波段;三槽梯形;耦合腔慢波结构;冷测

中图分类号:TN214 **文献标识码**:A

Introduction

W-band (75~110 GHz) is a particularly important area for emerging applications, such as high-data-rate communications, high-resolution radar and active imaging, which require high gain and broadband amplifiers with high power levels [1-2]. As a key device, the amplifier critically determines the performance of the whole elec-

Received date: 2019- 08- 03, **revised date**: 2019- 12- 02 **收稿日期**:2019- 08- 03,**修回日期**:2019- 12- 02

Foundation items: Supported by the Key Laboratory Foundation (614280701020117), China Postdoctoral Science Foundation (2017M62299)

Biography: LU Zhi-Gang(1981-), male, Chengdu, China, Ph. D. Research area involves terahertz traveling wave amplifier. E-mail: lzhgchnn@uestc. edu. cn

tronic systems. Due to its outstanding combined performance in power capacity and bandwidth, traveling wave tube (TWT) is one of the most important millimeter wave amplifiers [3-11]. Slow wave structure (SWSs) is the key component of TWT amplifier, facilitating efficient interaction between the electromagnetic wave supported by the structure and the electron beam.

In recent years, folded waveguide (FW) SWS was widely used in the *W*-band broadband TWT amplifier, and the state-of-the-art output power is more than 250 W in the frequency range of 89.6~97.6 GHz (8 GHz), with a maximum power of ~424 W and electronic efficiency of ~10% at 92.9 GHz, with beam current of 189-mA and beam voltage of 22.5-kV [12]. However, the further increase of output power is severely limited by the current that can be propagated through the device at this voltage, by the power loading on the circuit, and by issues of the circuit stability. Distributed beams, i.e., multiple or sheet beams, offer the prospect of significantly higher electron current, and hence power, with no increase in the operating voltage. Double-staggered-grating (DSG) SWS for sheet beam was proposed and used in the sheet beam TWT amplifier in *W*-band. At present, the state-of-the-art output power approaches 644 W at 94 GHz with a corresponding gain of 38.1 dB[13]. Both FW-SWS and SDG-SWS have the characteristics of all-metal, ease fabricated, low operating voltage, but the fatal obstacle is that the low interaction impedance limits the further improvement of output power.

In order to obtain higher output power, a sheet beam CC-SWS, called three-slot-staggered-ladder CC [14-16], was applied to W-band TWT for the first time. Three-slot-staggered-ladder CC-SWS had been shown to strike a good balance between high power and broadband capability. A generic design for one cell of the structure is shown in Fig. 1. It consists of two rectangular half cavities separated by a septum with a beam tunnel and three coupling slots; the cavity is constructed without ferrules. The adjacent cells are rotated 180° around the beam-tunnel axis (which is the same as being mirrored the long way) so that the beam tunnel stays in the same position and Slot 2 of the next cell is on the right side of the beam tunnel (looking down along the direction of electron travel). From the Fig. 1, the size of CC-SWS is so small that it cannot be machined by the integrated fabrication technology which is mainly used to fabricate FW-SWS and SDG-SWS. So the single metal-diaphragm of three-slot-staggered-ladder CC-SWS, as shown in Fig. 1(b), is firstly machined by the high-precision CNC milling, and then assembled and welded under the microscope. What we have to pay special attention to here is that cumulative errors caused by diaphragm-assembly must be considered. So far the experimental study on a *W*-band three-slot-staggered-ladder CC-TWT circuit has not been reported. In this paper, we discuss the fabrication technology and cold-test according to the simulation results of the three-slot-staggered-ladder CC-SWS, which is the first demonstration of the application of sheet beam CC-SWS in W-band TWT.

1 Design and simulation

The dispersion and interaction impedance of the sheet beam CC-SWS with parameters listed in Table 1 were obtained by the simulating method using the Ansoft HFSS. The fundamental harmonic of the first mode is backward wave for this type of circuit, so the first spatial harmonic is selected to interact with electron beam, as shown in Fig. 2(a). And an unconventional mode 2 appears in the dispersion diagram due to the introduction of wide sheet beam tunnel. In order to reduce mode competition, the electron beam tunnel must not be too wide. The normalized phase velocity versus frequency of the fundamental mode at the first spatial harmonic is also given in Fig. 2(b). It shows that the dispersion curve is relatively flat over a broad bandwidth. And the phase velocity determines the beam voltage, which is approximately

Table 1 Parameters for simulated SWS
表1 慢波结构的参数

Parameter	mm
Period	1.2
Slot 1 & 2 width	0.25
Slot 1 & 2 length	1.22
Slot 3 width	0.3
Slot 3 length	1.42
Cavity width	2.32
Cavity height	1.22
Beam tunnel	
width	1.2
height	0.30
Diaphragm thickness	0.32

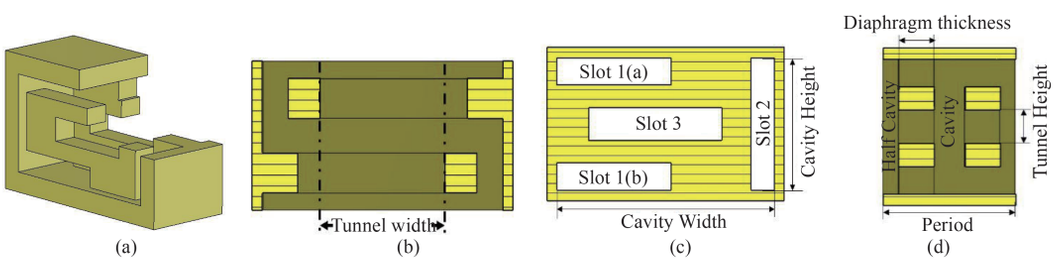

Fig.1 (a) Cut-away isometric view of a 3-D model of a full period (created by stacking two rotated unit cells), (b) the top view, (c) the left view, and (d) the front view of cutting-plane of the full period three-slot SWS
图1 (a) 全周期三维模型的等距剖视图 (b) 顶视图, (c) 左视图, (d) 前视图

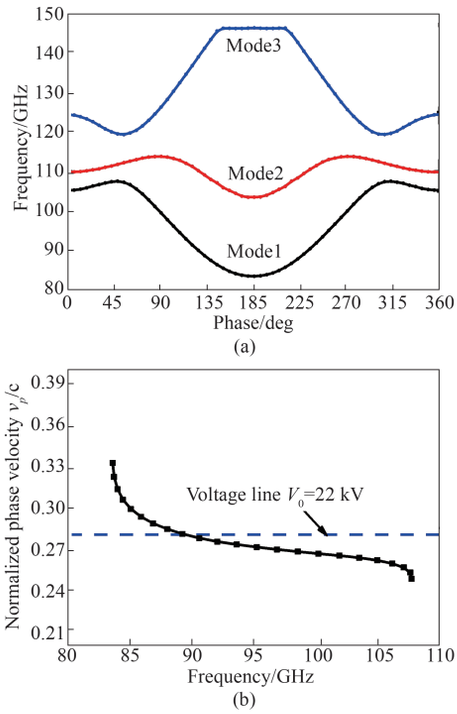

Fig.2　Dispersion curves of the sheet beam CC-SWS (a) frequency varies with phase shift, (b) normalized phase velocity varies with frequency

图2　带状注耦合腔慢波结构的色散曲线 (a) 频率随相移的变化, (b) 归一化相速随频率的变化

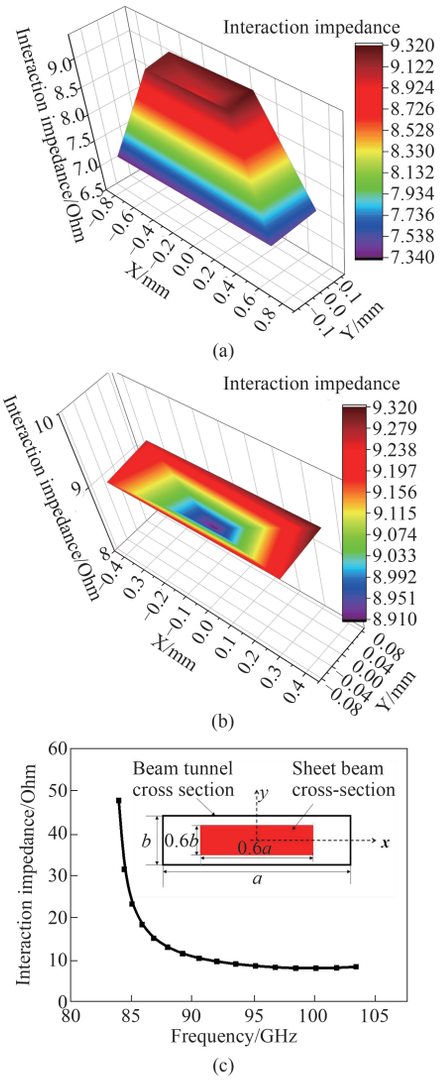

Fig.3　The distribution of interaction impedance on (a) the cross-section of beam tunnel, (b) the cross-section of sheet beam, and (c) average interaction impedance over the cross-section of sheet beam

图3　(a) 耦合阻抗在电子注通道上的分布, (b) 耦合阻抗在电子注截面上的分布, (c) 电子注截面上的平均耦合阻抗

22 kV here, required for synchronized interaction with the electron beam.

As a measure of the beam-wave interaction strength, the interaction impedance over cross-section of the sheet beam is also calculated using the Ansoft HFSS. First, the distribution of interaction impedance on the cross-section of beam tunnel is analyzed, and given as shown in Fig. 3(a). Secondly, according to the distribution of interaction impedance on the cross-section of sheet beam in Fig. 3(b), the position and size of electron beam are determined, and the average interaction impedance on the cross-section of sheet beam is calculated and shown in Fig. 3(c). Compared with the CC-SWS using the circular electron beam, the interaction impedance is basically at the same level [17], and the interaction impedance of three-slot-staggered-ladder CC-SWS is much higher than that of the FW-SWS and SDG-SWS [12-13]. The sheet beam can increase the DC input power by distributing the beam current over an increasing area, which indicates that the sheet beam CC-TWT can obtain higher output power.

Impedance matching between the CC-SWS and input-output waveguide is important for signal transmission, which can improve tube efficiency, gain and stability over the required bandwidth. The transmission model of the sheet-beam CC-SWS including the main section, input/output couplers and RF windows is present, as shown in Fig. 4(a). The coupler is a three-order step-transform rectangular waveguide placed on the short edge of the input/output cavity. The optimal design of coupler for sheet-beam CC-SWS is obtained using the time-domain solver in the CST Microwave Studio. The simulation results of transmission characteristics are given in Fig. 4(b). The reflection parameter S_{11} is almost below −20 dB in the frequency range of 91.2~100.7 GHz.

A 3-D particle-in-cell (PIC) model of sheet-beam CC-TWT is constructed. The beam-wave interaction simulations are carried out by using the PIC solver in CST Particle Studio to substantiate the amplification capability of the TWT. In the simulation, the cross-section size of sheet beam is set as 0.72 mm×0.18 mm. The synchronous voltage is 22 kV and the current of 500 mA. According to the beam tunnel size of 1.2 mm×0.3 mm, the filling ratio is 36% (60% in both x- and y-coordinates), then the current density of sheet beam is 379 A/cm^2. In order to make the sheet beam propagate stably and not be intercepted by the slow wave circuit, a 0.8 Tesla uniform

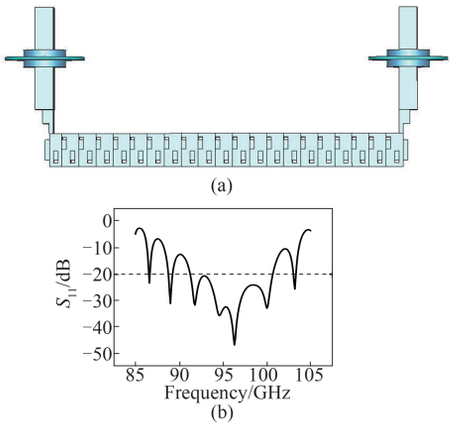

Fig.4 (a) The vacuum model, and (b) the transmission characteristics of the sheet beam CC-SWS
图4 (a) 带状注耦合腔慢波结构的真空模型, (b) 传输特性S_{11}计算结果

solenoidal magnetic field is used for beam focusing. In addition, it should be noted that the saturated gain of the whole TWT is low (less than 20 dB generally), so the length of the tube can be further shortened to ensure the stable transmission of the sheet beam with such high current density. In the following calculation, the saturated gain and length of sheet-beam CC-TWT are given. The material of SWS circuit is set as oxygen-free copper, and its conductivity is 2.25×10^7 S/m, which means the distribution loss and surface roughness of the circuit is considered. The typical simulation results at the center frequency of 94 GHz are exhibited in Fig. 5-8.

All of the electrons are well confined in the beam tunnel, with no electron intercepted, and the electron bunching phenomenon around the end of the circuit is given, as shown in Fig. 5. According to the Fig. 5, the accelerating electrons and retarding electrons are periodically arranged along the longitudinal direction, which demonstrates a good beam-wave energy exchange process. Fig. 6 shows the phase momentum plot of the bunched electron beam along the longitudinal distance when the electron dynamic system has been in steady state. As the electron beam propagates along the circuit, most of the electrons experience a continuous deceleration along the slow-wave circuit. This continuous interaction results in a continuously increasing wave amplitude at the output port of the TWT, as depicted in Fig. 7. The power at output port becomes stable at 1125 W, corresponding to the gain of 15.75 dB without oscillation. Fig. 8 gives the frequency spectrum of output signal. As for the output signal, the spectrum is relatively pure. Although the higher harmonics are also aroused, the amplitudes are much lower than that of the operating frequency of 94 GHz.

According to the same method, the TWT at each frequency can be driven to the saturated state by adjusting the input power. The plot of saturated output power versus frequency in the frequency range of 91~96 GHz is shown in Fig. 9(b). The designed sheet-beam CC-TWT can produce saturated output power of more than 1000 W

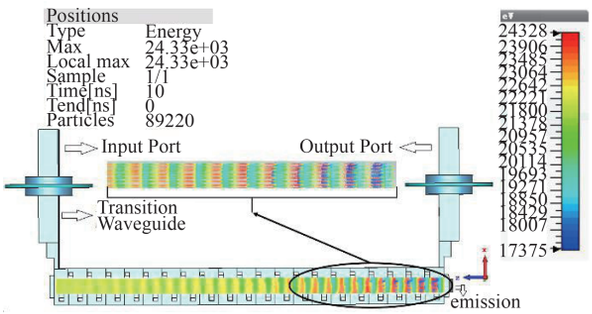

Fig. 5 The electron bunching phenomenon at 94 GHz
图5 94 GHz时的电子群聚图

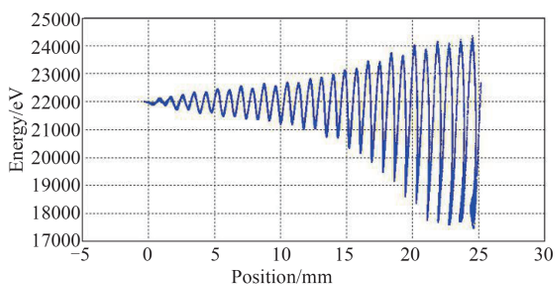

Fig. 6 Phase momentum of bunched electron beam at 94 GHz
图6 94 GHz时,群聚电子注的相空间图

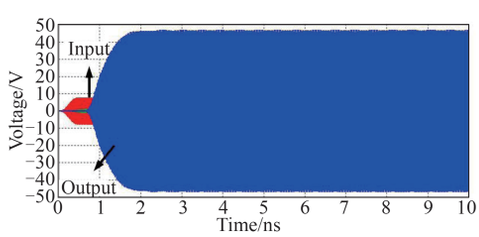

Fig. 7 Input and output signals at 94 GHz
图7 94 GHz时,输入输出信号图

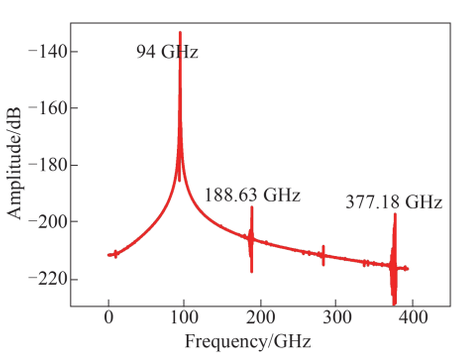

Fig. 8 Frequency spectrum of output signal at 94 GHz
图8 94 GHz时,输出信号的频谱图

in the frequency range of 91~96 GHz, and the corresponding saturated gain can reach over 15 dB. The maximum saturated output power can reach 1125 W at 94 GHz. The saturated electron efficiency is greater than 8.52% across the frequency range of 91~96 GHz.

2 Fabrication and cold-test

The W-band three-slot-staggered-ladder CC-TWT

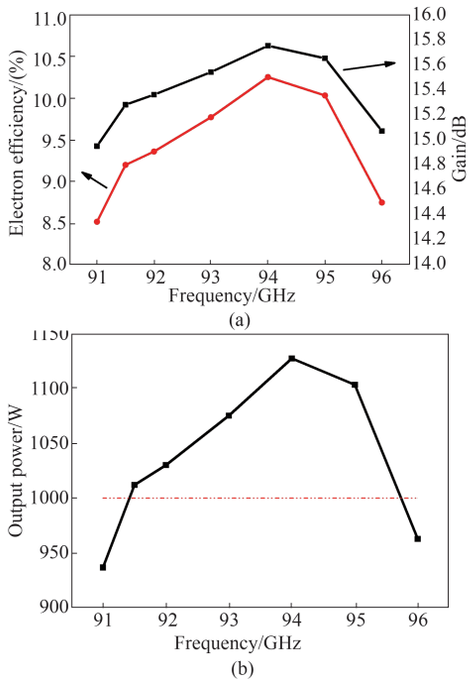

Fig. 9　(a) The electron efficiency and saturated gain, and (b) the saturated output power versus the frequency
图 9　(a) 电子效率和饱和增益随频率的变化, (b) 饱和输出功率随频率的变化

circuit was fabricated by using the traditional machining method, where the circuit is milled by a micromachining high speed CNC mill. The size of the CC-diaphragm is 2.32 mm×1.22 mm, and three grooves as well as the beam tunnel are opened on the diaphragm. The structural dimensions are very small, and it is difficult to fabricate using the common oxygen-free copper. Here the special oxygen-free copper is used to fabricate the diaphragm. Meanwhile in order to reduce the superposition error, the accuracy of each coupled-cavity diaphragm thickness is strictly controlled within a certain range. Each piece is numbered and assembled in order. The fabricated coupled-cavity diaphragms, transition waveguides and input & output window components are shown in Fig. 10.

Fig. 10　(a) Coupled-cavity diaphragms, (b) transition waveguides, and (c) input & output window components
图 10　(a) 耦合腔膜片, (b) 转换波导, (c) 窗组件

To test the transmission characteristics of the W-band three-slot-staggered-ladder CC-TWT circuit, the clamping molds are designed to assemble and fix the components of the CC-SWS diaphragms. The test sample is shown in Fig. 11. For the CC-SWS (20 cycles) tested in

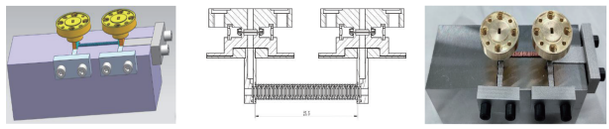

Fig. 11　(a) Clamping molds and the final test sample, (b) assembly drawing using UG software, and (c) assembly for testing
图 11　(a) 夹具和测试模型, (b) 在 UG 软件中的组装示意图, (c) 组装与测试

this paper, the measured cumulative error is 0.06 mm (the machining accuracy is 0.005 mm, the maximum cumulative error is 0.1 mm).

Figure 12 shows the test site. The Vector Network Analyzer (VNA) is used to test the *S* parameters and voltage standing wave ratio (VSWR) of three-slot-staggered-ladder CC-TWT circuit. Here, two 90-degree bend-waveguides are used to connect to two *S*-parameter spread spectrum modules of VNA, respectively. The test result of the parameter S_{11} is shown in Fig. 13, which shows that magnitude of reflection signal is less than -10 dB over the frequency range of 90~100 GHz. According to the test results, the VSWR is deduced and shown in Fig. 14. At the same time, as a comparison, the simulation results of S_{11} and VSWR are also plotted on the Fig. 13 and Fig. 14. It can be seen that the simulation results are not in good agreement with the test results. For *W*-band SWS, the machining accuracy of 0.005 mm is far enough to meet the manufacturing requirements. The errors of simulation and test results are mainly caused by assembly and welding. Assembly error is inevitable and can only be improved by the technology of technicians. For the welding, only the I/O waveguide is welded, the coupled-cavity diaphragms are too small to be welded, so the mold is used to fix them, as shown in Fig. 11. The electromagnetic wave can leak out through the tiny gap between the coupled-cavity diaphragms, which is the main reason for the error between the test and simulation results. In the future, a stainless steel sleeve can be used to seal the diaphragms, which is an effective way to solve the welding error.

Fig. 12　Test site of the CC-TWT circuit
图 12　耦合腔行波管电路的测试现场

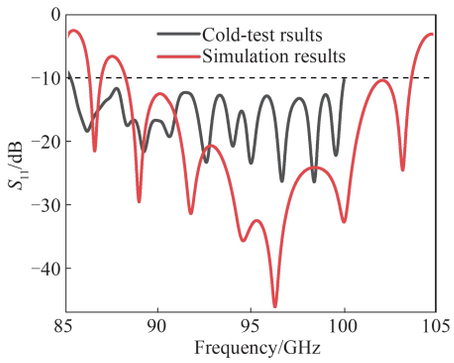

Fig. 13 S_{11} comparison between cold-test and simulation results
图13 S_{11}冷测结果和模拟结果的比较

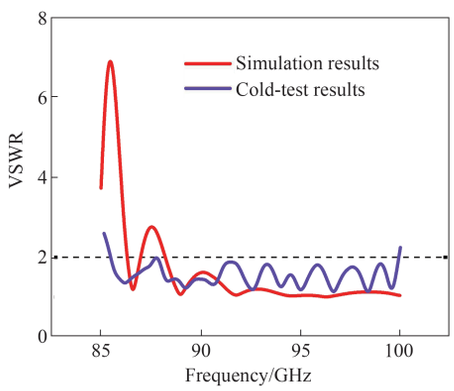

Fig. 14 VSWR comparison between test and simulation results
图14 VSWR冷测结果和模拟结果的比较

3 Conclusion

The design of sheet beam CC-TWT with a single-section SWS was carried out. The piece parts of three-slot-staggered-ladder CC-SWS, couplers and RF windows were fabricated and assembled. Cold tests were carried out to characterize the three-slot-staggered-ladder CC-SWS and the RF windows. The measured *S*-parameter S_{11} is less than -10 dB in the frequency range of 90-100 GHz. These results lay the foundation for the realization of the W-band three-slot-staggered-ladder CC-TWT.

References

[1] Abrams R H, Levush B, Mondelli A A, *et al*. Vacuum electronics for the 21st century [J]. *IEEE Microwave Magazine*, 2001, **2**(3): 61-72.

[2] Booske J H, Dobbs R J, Joye C D, *et al*. Vacuum electronic high power terahertz sources [J]. *IEEE Transaction on Terahertz Science and Technology*, 2011, **1**(1): 54-75.

[3] Wang S M, Aditya S, Miao J, *et al*. Design of a sheet-beam electron-optical system for a micro fabricated W-band traveling-wave tube using a cold cathode [J]. *IEEE Transaction on Electron Devices*, 2016, **63**(9): 3725-3732.

[4] Fang S, Xu J, Yin H R, *et al*. Experimental verification of the low transmission loss of a flat-roofed sine waveguide slow-wave structure [J]. *IEEE Electron Device Letters*, 2019, **40**(5): 808-811.

[5] Lu Z, Ge W, Wen R, *et al*. High power folded waveguide traveling wave tube based on variable-width technology [J]. *Physics of Plasma*, 2019, **26**(5): 31061-31067.

[6] Cook A M, Joye C D, Calame J P. W-Band and D-Band traveling-wave tube circuits fabricated by 3D printing [J]. *IEEE Access*, 2019, **7**: 72561-72566.

[7] Srivastava A, Christie V L. Design of a high gain and high efficiency W-band folded waveguide TWT using phase-velocity taper [J]. *Journal of Electromagnetic Waves and Applications*, 2018, **32**(10): 1316-1327.

[8] Mineo M, Carlo A D, Paoloni C. Analytical design method for corrugated rectangular waveguide SWS THz vacuum tubes [J]. *Journal of Electromagnetic Waves and Applications*, 2010, **24**(17-18): 2479-2494.

[9] YANG Quan, ZHANG Lu-Qi, FANG Shuan-Zhu, *et al*. An optimal design of W-band truncated sine waveguide traveling wave tube [J]. *Journal of Infrared and Millimeter Waves*, (阳权, 张鲁奇, 方栓柱, 等. W波段平顶型正弦波导行波管的优化设计. **红外与毫米波学报**) 2018, **37**(2): 235-240.

[10] WANG Hai-Long, SHI Xian-Bao, WANG Zhan-Liang, *et al*. Research on W band step-type staggered double vane slow wave structure traveling wave tube [J]. *Journal of Infrared and Millimeter Waves*, (王海龙, 石先宝, 王战亮, 等. W波段阶梯型交错双栅慢波结构行波管的研究. **红外与毫米波学报**) 2018, **37**(6): 784-789.

[11] Malek F. The analytical design of a folded waveguide traveling wave tube and small signal gain analysis using Madey's theorem [J]. *Progress in Electromagnetics Research*, 2009, **98**(1): 137-162.

[12] Zhang X, Feng J, Cai J, *et al*. Design and experimental study of 250-W W-band pulsed TWT with 8 GHz bandwidth [J]. *IEEE Transaction on Electron Device*, 2017, **64**(12):5151-5156.

[13] Fan Y, Luo J, Fang Z. W-band sheet beam staggered double grating traveling wave tube with simplified input output structure: Proceeding of International Vacuum Electronics Conference, London, 2017 [C]. IEEE, 2017: 1-2.

[14] Larsen P B, Abe D K, Cooke S J, *et al*. Characterization of a Ka-band sheet beam coupled cavity slow wave structure [J]. *IEEE Transaction on Plasma Science*, 2010, **38**(6): 1244-1254.

[15] Pershing D E, Nguyen K T, Abe D K, *et al*. Demonstration of a wideband 10-kW Ka-band sheet beam TWT amplifier [J]. *IEEE transaction on Electron Devices*, 2014, **61**(6): 1637-1642.

[16] Su Z, Lu Z, Wang Z, *et al*. Preliminary design of a three-slot-staggered-ladder coupled-cavity structure for W-band pulse power traveling wave tube: Proceeding of International Vacuum Electronics Conference, Montery, 2018 [C]. IEEE, 2018: 131-132.

[17] Liu Y, Gong Y, Wei Y, *et al*. Design of a 100 W V-band coupled cavity traveling wave tube: China-Japan Joint Microwave Conference, Hangzhou, 2011 [C]. IEEE, 2011: 458-460.